Published: 7th October 2026

ANACHEM JOURNAL
ISSN: 2006-5221 (Online)

SONOCHEMICAL SYNTHESIS AND PRELIMINARY PHOTOCATALYTIC EVALUATION OF A RU–TCPB COORDINATION MATERIAL FOR CONGO RED DECOLORIZATION

[*1]Omosun, N.N., [1]Odih, C., [1]Chukwuemeka-Okorie, H.O., and [1]Emeremnu, E.M

[1]Department of Pure and Industrial Chemistry, Michael Okpara University of Agriculture, Umudike, Abia State, Nigeria
*Corresponding author's email: omosun.nike@mouau.edu.ng, ORCID ID: 0000-0001-8707-2805
https://doi.org/10.5281/zenodo.23130363

ABSTRACT

A ruthenium-based coordination material (Ru-TCPB) was synthesized via a sonochemical approach from Ru(III) chloride and 1,2,4,5-tetrakis(4-carboxyphenyl)benzene (H_4TCPB) in dimethylformamide (DMF). The synthesized material was characterized using a range of analytical techniques, including Fourier transform infrared spectroscopy (FT-IR), UV–Vis spectroscopy, powder X-ray diffraction (PXRD), and scanning electron microscopy (SEM). The FT-IR spectrum of the Ru-TCPB shows shifts in absorption bands due to coupling with Ru compared to uncoordinated H_4TCPB. The UV–Vis spectrum of the Ru-TCPB exhibited a maximum absorption peak at 240 nm, corresponding to an optical band gap of 5.17 eV. The SEM images showed a microporous surface structure with aggregated morphology composed of irregularly shaped particles. The photocatalytic efficiency of the synthesized Ru-TCPB was evaluated for decolorizing Congo red, a widely used textile dye commonly found in industrial effluents. The photocatalytic performance was evaluated using a 50 mg/L Congo Red solution, with 0.05 g of catalyst dispersed in 20 mL of dye solution (2.5 g/L), and subsequently exposed to UV light irradiation and sunlight. Ru-TCPB showed excellent photocatalytic activity, achieving 100% decolorization based on absorbance at 560nm after 120 min of UV irradiation and 65% under natural sunlight. Kinetic studies revealed that the decolorization process follows a pseudo-first-order reaction model. The results show the potential of the Ru-TCPB as an effective photocatalyst material for degrading Congo red dye in water.

Keywords: Ruthenium; coordination material; photocatalytic decolorization; sonochemical synthesis.

1.0. Introduction

Ultrasound (sonochemical) synthesis of coordination materials has emerged as a preferred route because it is rapid, energy-efficient, and cost-effective. This method provides sufficient energy to promote efficient nucleation under relatively mild reaction conditions, producing materials with desirable physicochemical properties, unlike conventional solvothermal methods, which often require elevated temperatures, extended reaction times, and substantial solvent use (Carson et al., 2011). These coordination materials synthesized through sonochemical methods have been used for various environmental applications such as wastewater treatment, gas capture, and photocatalytic degradation of pollutants. (Yap et al., 2017). Among organic contaminants, synthetic dyes are of particular concern because they are widely

used in most manufacturing industries. Synthetic dyes have complex molecular structures, are poorly biodegradable, and are highly stable. Synthetic dyes largely resist conventional biological treatment processes, allowing them to persist in aquatic systems for long periods and pose environmental risks and health hazards. (Periyasamy, 2024, Kumar et al., 2025). Synthetic dyes in water bodies not only reduce light penetration and dissolved oxygen levels. They also generate toxic and potentially carcinogenic by-products. These issues therefore call for reliable and efficient remediation technologies.

1-Naphthalenesulfonic acid, 3,3′-(4,4′-biphenylenebis (azo)) bis (4-amino-) disodium salt, also known as Congo red, is a synthetic anionic azo dye often used in the manufacturing of rubber and printing industries (Mandal et al., 2021). Congo red in water bodies can impair water quality and inhibit photosynthetic activity, even at relatively low concentrations. This can adversely affect aquatic organisms. Therefore, effectively removing or degrading Congo red dye from water is an important environmental challenge (Oladoye et al., 2022). Several treatment methods, such as adsorption, membrane filtration, coagulation/flocculation, and advanced oxidation processes, have been studied for dye removal in wastewater (Mahlambi et al., 2015). However, these techniques often have limitations, including incomplete mineralization, secondary waste generation, high operational costs, limited regeneration efficiency, and poor performance against resistant organic pollutants (Martínez-Huitle et al., 2023).

Photocatalysis has been reported as an alternative approach to address these issues. It allows for the complete oxidation of organic contaminants under mild operating conditions, and photocatalysis may achieve partial transformation, decolorization, or mineralization depending on the catalyst and operating conditions (Mohamadpour & Amani, 2024). A photocatalyst material generates electron-hole pairs that produce reactive oxygen species upon light irradiation, such as superoxide and hydroxyl radicals. These radicals effectively degrade complex organic compounds into carbon dioxide, water, or inorganic ions. (Banerjee et al., 2014).

Coordination materials are a broad class of materials formed by coordinating metal ions with ligands to form discrete complexes, extended networks, or porous structures. These include discrete coordination complexes, coordination polymers, metal-organic frameworks, and porous coordination polymers. These materials have attracted considerable attention because of their structural versatility, tunability, and unique physicochemical properties (Yasin et al., 2024). These characteristics make coordination materials promising for a wide range of applications, including gas adsorption and storage, catalysis, chemical sensing, drug delivery, and energy storage (Tian et al., 2025). More recently, some coordination materials have emerged as promising photocatalysts because of their redox activity, light-absorbing ability, ability to facilitate charge separation and transfer, and accessible active sites for photocatalytic reactions (Hornberger & Adams, 2022).

Ruthenium compounds have demonstrated considerable potential as light-harvesting materials because of their favorable electronic structure, chemical stability, redox activity, and efficient charge-transfer processes, and their application as sustainable photocatalysts for water decontamination has been reported (Al-Temimei, 2024; Zhang et al., 2023). This study aims to contribute to the existing body of knowledge by expanding the range of ruthenium-based coordination materials investigated for photocatalytic water treatment and by demonstrating the

feasibility of a sonochemical approach for their synthesis.

In this study, we focused on 1,2,4,5-tetrakis(4-carboxyphenyl)benzene (H_4TCPB), a tetratopic organic linker scaffold, and ruthenium metal. The key features of H_4TCPB are: (i) it provides a sufficient conjugated π-electron system that promotes charge delocalization; (ii) it acts as the light-harvesting organic chromophore; (iii) it enables the formation of microporous channels that may enhance adsorption of dye molecules and dissolved oxygen near active metal sites. Also, including transition metals such as ruthenium can further enhance photocatalytic performance through improved redox activity and efficient charge-transfer processes (Al-Temimei, 2024). To the best of our knowledge, no study has reported combining a ruthenium–TCPB coordination framework, sonochemical synthesis, and its application for Congo red photodecolorization. Here, we synthesized a ruthenium-based coordination material via a sonochemical approach and characterized it using spectroscopic and analytical techniques. We investigated the photocatalytic decolorization performance of Ru-TCPB on Congo red under light irradiation, with particular emphasis on decolorization efficiency and reaction kinetics.

2.0. Materials and Methods

1,2,4,5-Tetrakis(4-carboxyphenyl)benzene (H_4TCPB) and ruthenium chloride were purchased from Sigma-Aldrich. Analytical-grade Congo Red (97% purity) was obtained from Molychem and used without further purification. Solvents were purchased from Bristol Scientific, Nigeria. Ru-TCPB was synthesized using an Elementrix ultrasonicator. Infrared (IR) absorption spectra were recorded with a Nicolet IS20 FT-IR spectrometer using attenuated total reflectance (ATR). X-ray diffraction (XRD) data were collected using a Thermo Scientific Companion diffractometer. Surface morphology was assessed using an Axia ChemiSEM (Thermo Scientific), while UV-visible analysis was conducted with a Cary 60 (Agilent) UV spectrophotometer.

2.1. Synthesis of Ru-TCPB via Ultrasonic Irradiation

The Ru-TCPB coordination material was synthesized following the method described by Saidi et al. (2020) with modifications. Ruthenium(III) chloride ($RuCl_3$, 2.07 g, 10 mmol) and 1,2,4,5-tetrakis(4-carboxyphenyl)benzene (H_4TCPB) ($C_{34}H_{22}O_8$, 2.15 g, 10 mmol) were used in DMF, as shown in Figure 1 below.

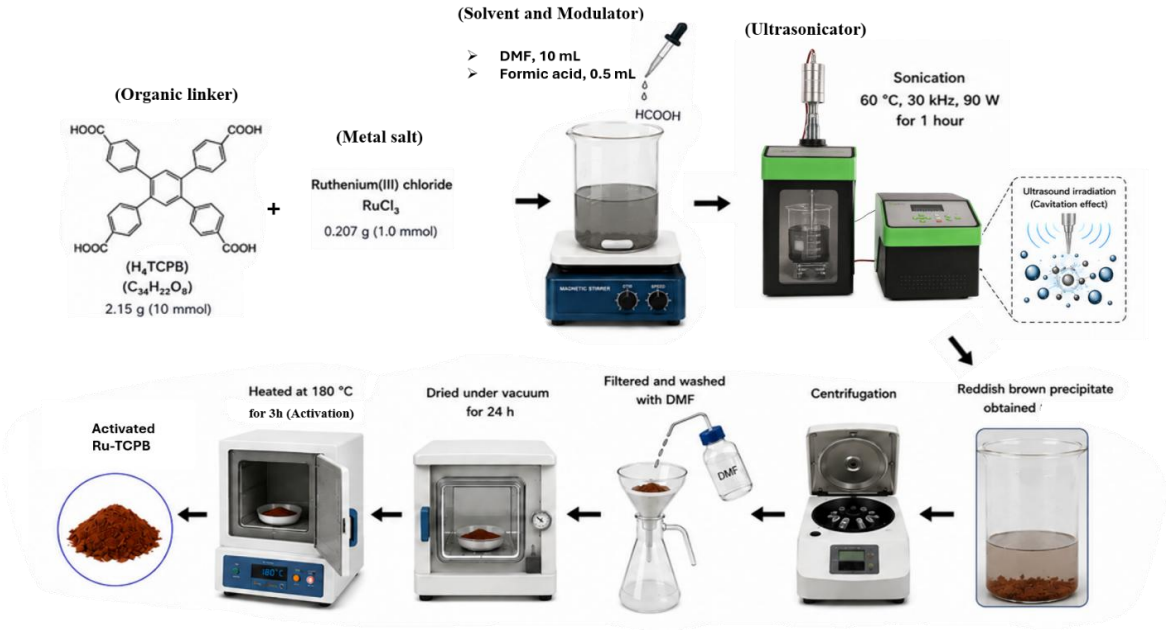

Figure 1: Schematic flow process for the synthesis of Ru-TCPB

The compounds were dissolved in dimethylformamide (DMF, 10 mL), and formic acid (0.5 mL, AR 98.0%) was used as a modulating agent. The resulting solution was stirred magnetically for 30 minutes to ensure homogeneity. The mixture was transferred to an ultrasonic reactor and treated at 60 °C, 30 kHz, and 90 W for 1 hour. The resulting reddish-brown precipitate was isolated by centrifugation at 3000 rpm for 10 min. After centrifugation, the supernatant was carefully decanted and discarded. The residue was filtered under vacuum and washed three times with 10 mL DMF to remove unreacted species. The product was dried under vacuum for 24 hours and heated at 180 °C for 3 hours to obtain an activated sample.

2.2. Photocatalytic decolorization of Congo red dye procedure

The photocatalytic decolorization of Congo red was investigated using the synthesized coordination material as the photocatalyst. Prior to the experimental analysis, a calibration curve for Congo red was established using standard solutions in the concentration range of 5–50 mg/L. Absorbance measurements at 560 nm showed a linear relationship with concentration ($R^2 = 0.998$), which was used to determine Congo red concentration in the experimental samples. For the photocatalytic decolorization procedure, a 50 mg/L aqueous Congo red solution was prepared as the initial dye concentration, and the initial pH was measured at 6.8 without any pH adjustment. For each experiment, 0.05 g of catalyst (2.5 g/L) was dispersed in 20 mL of Congo red solution in a Pyrex glass beaker. The suspension was stirred in the dark for 20 min at room temperature, then irradiated under UV light or sunlight with constant magnetic stirring. After the desired time, the mixture was centrifuged at 5000 rpm for 10 min and filtered through Whatman No. 1 filter paper to remove catalyst particles before measuring absorbance at 560 nm using a UV-Vis spectrophotometer**.** The procedure was based on the method of Khan et al. (2022) with minor modifications.

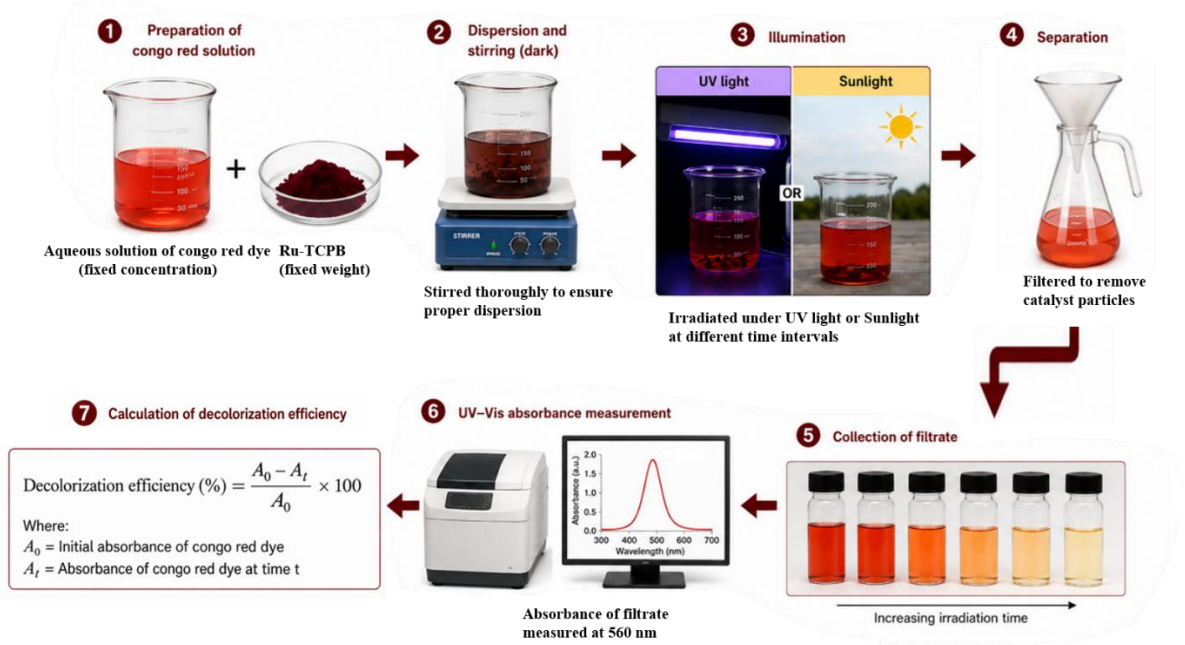

Figure 2: Schematic presentation of photocatalytic procedure

The photocatalytic decolorization efficiency in percentage was calculated following a similar method reported by Abraham et al. (2016), using the formula:
Decolorization efficiency

$$(\%) = \frac{A_O - A_t}{A_O} \times 100 \quad \text{.....(1)}$$

where A_0 = absorbance before illumination, A_t = absorbance after illumination time.
The effect of irradiation time was studied at 15, 30, 60, and 120 minutes with 0.05 g of catalyst, while the effect of photocatalyst dosage (0.02 g, 0.04 g, 0.06 g, 0.08 g, and 0.10 g) for 30 minutes of irradiation time on dye decolorization was evaluated.

3.0. Results and Discussion

3.1. Infrared Spectroscopy of Ru-TCPB

The FT-IR spectrum of Ru-TCPB in Figure 3 shows several distinct peaks in the 400–4000 cm^{-1} region. Table 1 provides peak assignments and positions.

Table 1: Peak assignments and their interpretations

Wavenumber (cm^{-1})	Assignment	Interpretation
3600–3000	Broad peak (O–H stretching)	Likely due to adsorbed moisture or uncoordinated carboxylic acids.
1680–1720	C=O stretching (free COOH)	Some peaks in this region (e.g., 1683, 1695 cm^{-1}) suggest presence of non-coordinated carboxyl groups from TCPB.

1550–1600	Asymmetric COO^- stretch	Coordination of carboxyl groups with Ru ions. E.g., 1580, 1609 cm^{-1}.
1400–1450	Symmetric COO^- stretch	Confirms carboxylate binding; this and the above together support metal–ligand coordination.
1000–1300	C–O and C–C aromatic bending	Vibrations within the TCPB aromatic ring framework.
600–800	M–O or M–C bonds (Ru–O)	Peaks at 672.47 cm^{-1} corresponds to Ru–O stretching.

The appearance of both asymmetric and symmetric carboxylate stretching bands confirms the coordination of TCPB's carboxyl groups to the Ru metal centers. The disappearance or weakening of the free carboxylic acid C=O peak (1700 cm^{-1}) compared to the spectrum of the pure organic linker indicates deprotonation and coordination to metal nodes. Peaks below 800 cm^{-1} are associated with Ru–O bonding, further confirming material formation (Hadjiivanov et al., 2020). Overall, the FT-IR data support successful coordination and interaction between the Ru metal and the organic linker.

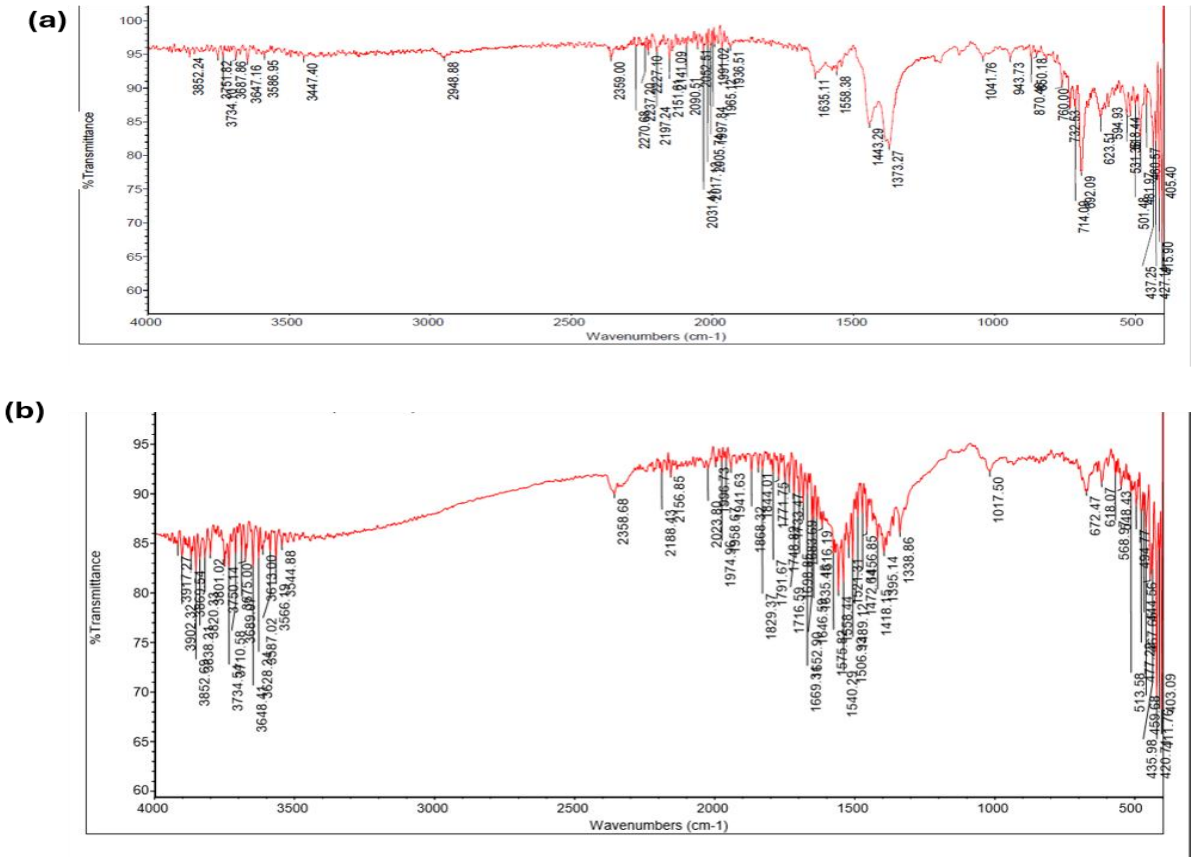

Figure 3: FT-IR spectrum of (a) free H_4TCPB and (b) Ru-coordinated TCPB

3.2. Ultraviolet – Visible Spectroscopy

The UV visible spectrum (range: spectrum (200–1100 nm) of the synthesized coordination material.

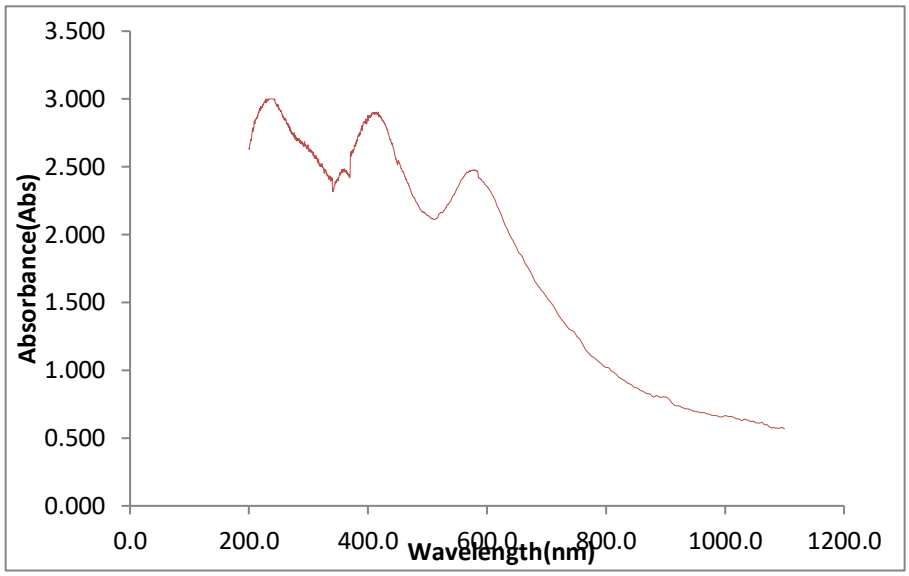

Figure 4: UV–Vis spectrum of the synthesized Ru-TCPB

The spectrum shows strong and broad absorptions in the UV and visible regions, indicating a complex electronic structure. Based on band gap values, a material can be classified as a conductor (very low band gap), an insulator (very large band gap), or a semiconductor (intermediate band gap) (Wang et al., 2019). In this work, the bandgap of the ruthenium organic framework was evaluated using the Planck's equation shown below (Fabrizio et al., 2022).

$$h\nu = \frac{hc}{\lambda\, max} \quad \text{.....(2)}$$

The symbols expressed in equation (2) are: E_g for band-gap energy, h for Planck's constant (6.626 x 10 $^{-34}$ J s), c for the speed (3 x 108 m s^{-1}), ν for the frequency and λ for wavelength of maximum Absorption (240 nm). Consequently, the bandgap (E_g) is evaluated as follows. Convert the wavelength to meters:

240 nm = 2.40 x 10^-7 m. Therefore:

$$E_g = \frac{(6.6261\times10^{-34}\ j.s)\times(3\times10^{8} m/s)}{2.40\times10^{-7} m} =$$

$$8.2825\ \times\ 10^{-19}\ J$$

Convert joules to electron volts:

$$E_g = \frac{8.2825\times10^{-19}}{1.602\ X\ 10^{-19}} = 5.17\ \text{eV}$$

The band gap of the Ru-TCPB is 5.17 eV.

From the plot, the wavelength of maximum absorption for the synthesized ruthenium organic framework was 240 nm. Generally, absorption between 200 and 400 nm is typical for ultraviolet (UV) radiation, while absorption between 400 and 800 nm represents visible light. Therefore, the observed absorption at 240 nm confirmed that the materials absorb maximally in the UV region. From visual inspection of the graph, the following spectral characteristics are noted in Table 2 below.

Table 2: Absorption peaks and assignment

Peak Wavelength (nm)	Approximate Absorbance (a.u.)	Possible Transition
240 – 280 nm	2.9 – 3.0	$\pi \rightarrow \pi^*$ transitions in the aromatic rings of TCPB
320 – 340 nm	2.4	$n \rightarrow \pi^*$ transitions (C=O groups in TCPB)
400 – 420 nm	2.8	Metal-to-ligand charge transfer (MLCT)
520 – 560 nm	2.2	d-d transitions in Ru(II) or ligand field transitions
620 – 700 nm	Decreasing absorbance	Extended MLCT tail or charge-transfer bands

3.3. X-ray Diffraction Analysis of Ru-TCPB

The XRD spectrum of the synthesized coordination material is shown in Fig. 5. It shows a broad distribution of peaks with no sharp, intense peaks. The spectrum shows broad and overlapping peaks between 5° and 30° in the 2θ range, with intensity gradually decreasing beyond 30°.

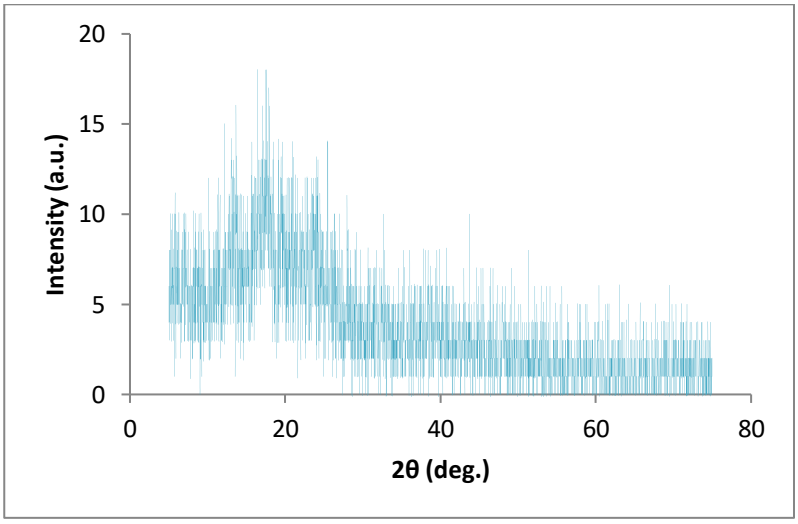

Figure 5: XRD plot of the synthesized Ru-TCPB.

Powder X-ray diffraction (PXRD) analysis of the synthesized coordination material was performed using Cu Kα radiation (λ = 1.5406 Å) over a 2θ range of (5–75°), with a step size of 0.02° and a scan rate of 2° min^{-1}. The X-ray tube was operated at 40 kV. No distinct or sharp Bragg peaks are observed, indicating poor crystallinity or an amorphous nature. The most intense region lies approximately between 10° and 25°; these broad peaks and lack of long-range order are characteristic of amorphous or semi-crystalline materials. (Bennett & Cheetham, 2014).

3.4. Scanning electron microscopy (SEM) of Ru-TCPB

SEM images at 100×, 500×, 1000×, and 2000× were taken at 5.00 kV in high-vacuum mode, revealing the surface morphology of the synthesized Ru-TCPB. At magnifications of 100x and 500x (lower magnification), an aggregated morphology composed of irregularly shaped particles was observed. This may suggest agglomeration. At magnifications of 1000x and 2000x (higher magnification), a more distinct surface texture was observed, revealing a pore array.

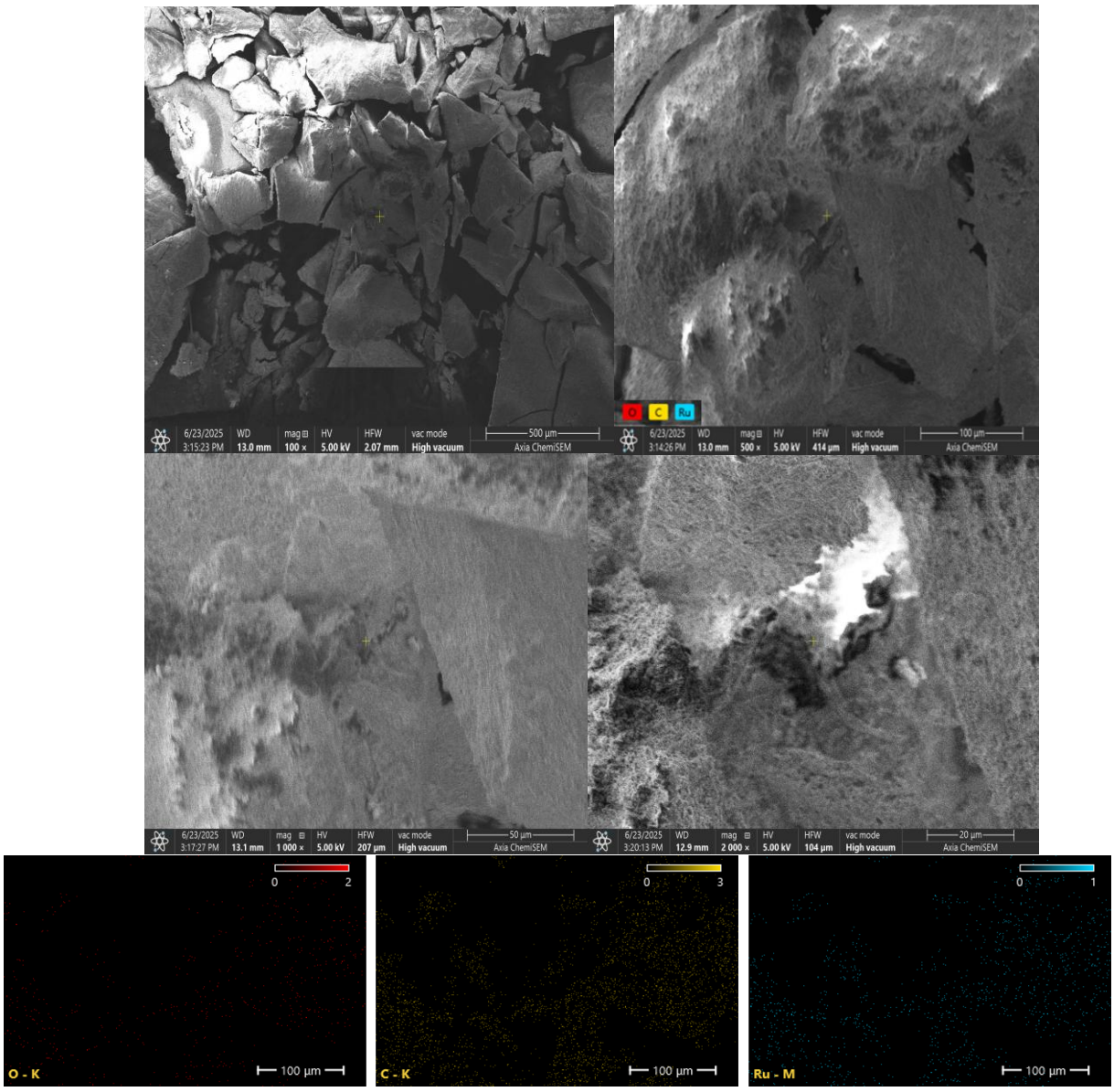

Figure 6: SEM image and elemental mapping of Ru-TCPB

3.5. Thermogravimetric analysis (TGA) of Ru-TCPB

TGA (Fig. 7) was used to evaluate the thermal stability of Ru-TCPB. The TGA thermogram shows a degradation profile at approximately 100 °C, likely due to the loss of physically adsorbed water or solvent molecules. Furthermore, weight loss was observed from 300 °C to 400 °C, which may be due to the loss of the organic linker or Ru-TCPB decomposition.

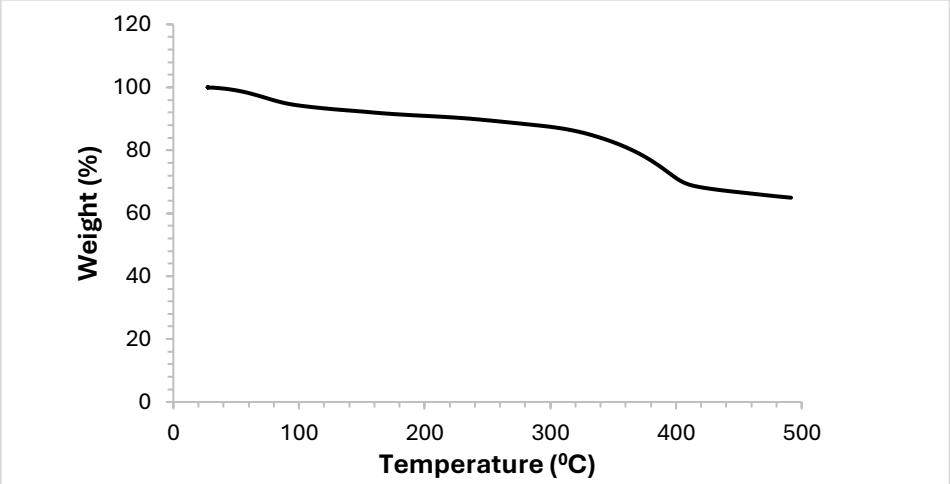

Figure 7: TGA Thermogram of Ru-TCPB

3.6 Photocatalytic decolorization of congo red using Ru-TCPB

3.6.1. Effect of time and photocatalyst dose

The decolorization of Congo red dye was carried out by light irradiation under UV irradiation and natural sunlight using a dosage of 0.05g of Ru-TCPB at different time intervals of 20 to 120 mins. The photocatalyst exhibited different performances under UV light and sunlight. The percentage decolorization of Congo red increases consistently with increasing irradiation time under both light sources. However, UV light showed higher decolorization efficiency, as shown in Fig. 8.

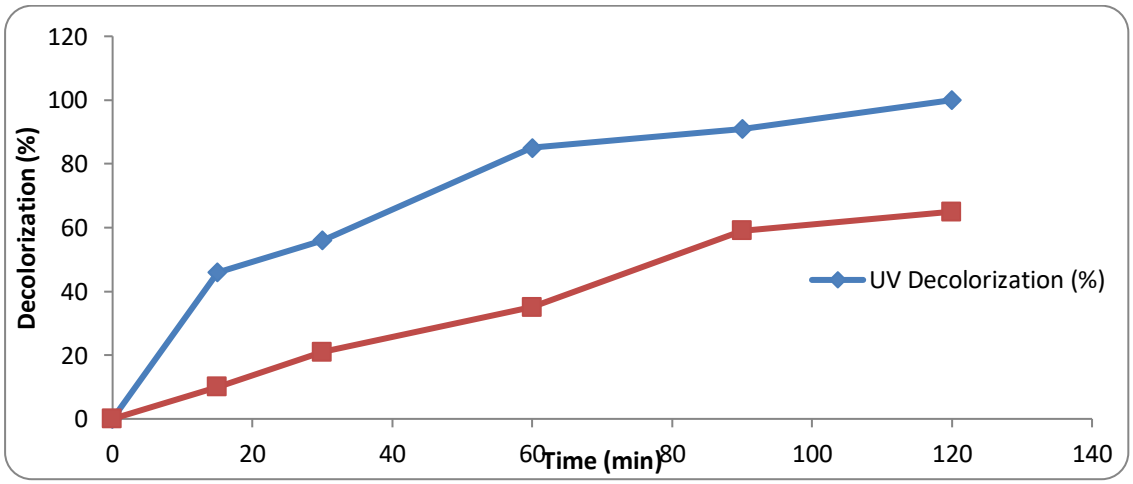

Figure 8: Comparison of percentage decolorization of Congo red dye under UV light and sunlight

Comparing the photocatalyst's decolorization efficiency under the two light sources, we observed 46% decolorization after 15 min under UV light, while 10% decolorization was observed under sunlight. This immediate difference shows that the catalyst responds effectively to the higher-energy photons provided by UV irradiation.

Overall, decolorization efficiency increased steadily with reaction time. As shown in Fig. 8, UV irradiation decolorization reached 56% after 30 min and increased to 85% in 60 mins. Decolorization rose further to 91% after 90 mins. However, under sunlight, the decolorization rate was lower at each interval, finally reaching 65% after 120 min. It is important to propose that under UV irradiation, the high photocatalytic performance observed may be attributed to the excitation of electrons from photo-induced ligand-to-metal, metal-to-ligand, or ligand-centered processes. UV photons also add sufficient energy to the Ru-TCPB band gap, generating more electron-hole pairs. These charged electrons react with adsorbed oxygen and water molecules to produce highly reactive oxygen species (ROS) such as hydroxyl radicals and superoxide radicals. (Mohamadpour and Amani 2024).

These radicals drive the oxidative decolorization of organic dye molecules, and increased production of these reactive radical species improves pollutant decolorization under UV light. In addition, the lower decolorization under sunlight may be attributed to the relatively small fraction of UV radiation in the solar spectrum possessing sufficient energy to excite the photocatalyst efficiently. Fewer charge carriers are generated, reducing ROS formation.

To estimate kinetic parameters, the decolorization was fitted to a pseudo-first-order kinetic model, which is commonly expressed as:

$$In\left(\frac{A0}{A}\right) = Kt \quad \text{..... (3)}$$

Since data are given as % decolorization efficiency (D), the remaining fraction is:

$$A0/_A = 1 - D \quad \text{..... (4)}$$

The working equation becomes:

$$In\left(\frac{1}{1-D}\right) = Kt \quad \text{..... (5)}$$

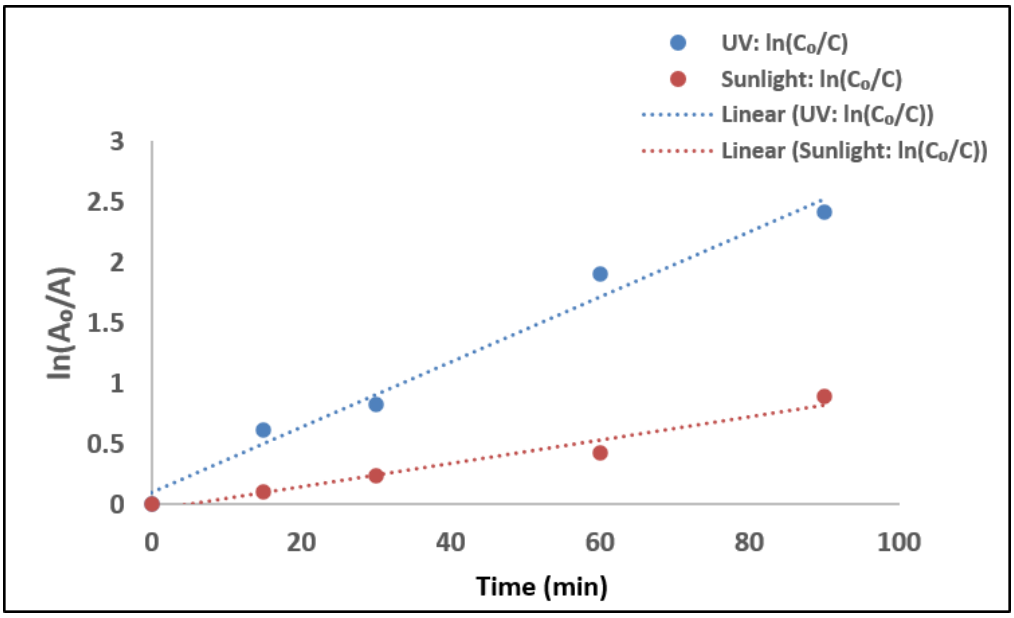

Figure 9: Kinetics of the decolorization process using Ru-TCPB

The pseudo-first-order kinetic analysis demonstrates that the photocatalytic decolorization follows a near-linear relationship between $\ln(A_0/A_t)$ and irradiation time for both UV and sunlight, with high coefficients of determination ($R^2 > 0.96$). The apparent rate constant under UV irradiation (0.0269 min^{-1}) is approximately 2.8 times greater than that obtained under natural sunlight (0.00955 min^{-1}). This confirms that the Ru-based coordination material exhibits substantially faster decolorization kinetics under UV light because the higher photon energy excites electrons across the band gap, generating a larger concentration of reactive oxygen species responsible for dye oxidation. The high regression values indicate agreement between the experimental data and the pseudo-first-order kinetic model, suggesting that photocatalytic decolorization is controlled by interactions between the dye molecules and photogenerated reactive species. The slightly higher regression value under UV irradiation (0.9802) compared with sunlight (0.9648) further suggests that the decolorization mechanism proceeds more consistently under controlled UV illumination than under natural sunlight, where fluctuations in solar intensity and spectral distribution may influence the reaction rate.

3.6.2 Effect of catalyst dosage on photocatalytic decolorization

The effect of Ru-TCPB photocatalyst dosage on Congo red decolorization was investigated by varying the catalyst dosage from 0.02 to 0.10 g for a fixed duration of 30 min. Fig. 10 shows the results. For the initial test, the decolorization investigation was carried out without the photocatalyst. No decolorization was observed under either UV or Sunlight. This confirms that the Ru-TCPB is indispensable for initiating the photocatalytic process. As the catalyst dosage increased, decolorization efficiency increased significantly under both irradiation sources. Under UV light, decolorization efficiency increased from 16% at a catalyst loading of 0.02 g to 26% at 0.04 g, then increased substantially to 55% at 0.06 g, with complete decolorization achieved at 0.08 g. After this, the results plateaued, suggesting that the optimum catalyst dosage under UV irradiation is approximately 0.08 g for a 20ml aqueous solution of Congo red.

For the sunlight irradiation, a similar trend was observed. The decolorization increased gradually from 5.4% at 0.02 g to 11% at 0.04 g, reaching 35% at 0.06 g and 65% at 0.08 g. A slight improvement to 71% was observed at 0.10 g, suggesting that the catalyst continued to benefit from additional active sites under sunlight. Increasing the catalyst loading also enhances light absorption by the photocatalyst, leading to the generation of more electron-hole pairs. Higher catalyst loading also increases active sites and potentially ROS generation, improving decolorization efficiency. These observations are consistent with previous reports on similar photocatalyst materials, where an optimum catalyst dosage balances active-site production with efficient light penetration. Beyond this, excessive catalyst loading can cause particle agglomeration or turbidity, which may scatter light and shield UV penetration into the reaction medium (Khan et al., 2022).

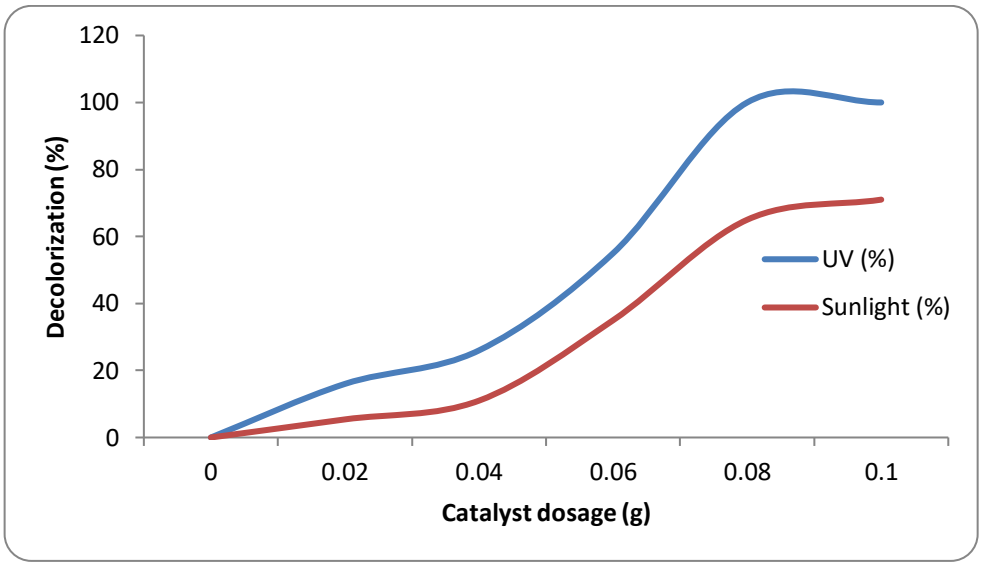

Figure 10. Percentage decolorization of Congo red at different catalyst dosages.

4.0 Conclusion

The Ru-TCPB was successfully synthesized through a straightforward sonochemical method using Ru(III) chloride and 1,2,4,5-tetrakis(4-carboxyphenyl)benzene (H_4TCPB) in DMF. The sonochemical route for synthesizing the ruthenium-based coordination material was facile, energy-efficient, and did not require harsh reaction conditions. The synthesized Ru-TCPB showed good photocatalytic performance for decolorizing Congo red.

Preliminary photocatalytic studies showed that UV irradiation produced substantially higher decolorization efficiencies, with complete decolorization achieved within 120 min. In natural sunlight, irradiation produced a decolorization efficiency of 65% over the same period. This indicates that the catalyst is more effectively activated by higher-energy UV photons, suggesting that UV-assisted photocatalysis is better suited for applications requiring rapid and complete pollutant removal. The catalyst's ability to function under natural sunlight, despite lower efficiency than UV irradiation, highlights its potential as an environmentally benign photocatalyst and a sustainable material for wastewater treatment using renewable solar energy. Further improvements through the organic linker, bandgap engineering, or mixed-metal doping may enhance its visible light response and increase its photocatalytic efficiency under solar irradiation.

Overall, these results demonstrate the potential of the Ru-TCPB as an effective photocatalyst material for treating dye-contaminated water. Important studies, such as the material's precise structure, its stability under irradiation, and possible Ru leaching, remain to be established. Future work will therefore focus on assessing catalyst stability, quantifying metal leaching, identifying degradation intermediates through TOC analysis, and evaluating recyclability. These studies will be essential for identifying the processes responsible for decolorization and assessing the material's practical potential for wastewater treatment.

Acknowledgment

This work was carried out with support from a grant under the UNESCO-TWAS programme, "Seed Grant for African Principal Investigators," financed by the German Ministry of Education and Research (BMBF). The views expressed

herein do not necessarily represent those of UNESCO-TWAS and BMBF. We gratefully acknowledge Engr. Akinboye Kunle of the Department of Metallurgical and Materials Engineering, University of Nigeria Nsukka, for his assistance with the scanning electron microscope and powder X-ray diffraction.

References

Abraham, S. D., David, S. T., Bennie, R. B., Joel, C., & Kumar, D. S. (2016). Eco-friendly and green synthesis of BiVO4 nanoparticles using microwave irradiation as a photocatalyst for the degradation of Alizarin Red. *Journal of Molecular Structure*, 1113: 174–181. https://doi.org/10.1016/j.molstruc.2016.01.053

Al-Temimei, F. A. (2024). The Ruthenium Metal Complexes and their Applications as a Light-Absorbing Material/ A DFT study. *Journal of Cluster Science,* 35(7): 2283–2291. https://doi.org/10.1007/s10876-024-02657-2

Banerjee, S., Pillai, S. C., Falaras, P., O'Shea, K. E., Byrne, J. A., & Dionysiou, D. D. (2014). New Insights into the Mechanism of Visible Light Photocatalysis. *The Journal of Physical Chemistry Letters*, 5(15): 2543–2554. https://doi.org/10.1021/jz501030x

Bennett, T. D., & Cheetham, A. K. (2014). Amorphous Metal–Organic frameworks. *Accounts of Chemical Research*, 47(5): 1555–1562. https://doi.org/10.1021/ar5000314

Carson, C. G., Brown, A. J., Sholl, D. S., & Nair, S. (2011). Sonochemical Synthesis and Characterization of Submicrometer Crystals of the Metal–Organic Framework. *Crystal Growth & Design*, 11(10): 4505–4510. https://doi.org/10.1021/cg200728b

Fabrizio, K., Le, K. N., Andreeva, A. B., Hendon, C. H., & Brozek, C. K. (2022). Determining optical band gaps of MOFs. ACS Materials Letters, 4(3): 457–463. https://doi.org/10.1021/acsmaterialslett.1c00836

Hadjiivanov, K. I., Panayotov, D. A., Mihaylov, M. Y., Ivanova, E. Z., Chakarova, K. K., Andonova, S. M., & Drenchev, N. L. (2020). Power of Infrared and Raman Spectroscopies to Characterize Metal-Organic Frameworks and Investigate Their Interaction with Guest Molecules. *Chemical Reviews*, 121(3): 1286–1424. https://doi.org/10.1021/acs.chemrev.0c00487

Hornberger, L., & Adams, F. (2022). Photocatalytic CO2 conversion using Metal-Containing coordination polymers and networks: Recent developments in material design and mechanistic details. *Polymers,* 14(14): 2778. https://doi.org/10.3390/polym14142778

Khan, S., Noor, A., Khan, I., Muhammad, M., Sadiq, M., & Muhammad, N. (2022). Photocatalytic degradation of organic dyes contaminated aqueous solution using binary $CdTiO_2$ and ternary $NiCdTiO_2$ nanocomposites. *Catalysts,* 13(1): 44. https://doi.org/10.3390/catal13010044

Kumar, M., Singh, V. P., Bhat, S. B., & Kumar, R. (2025). Environmental risks of textile dyes and photocatalytic materials for sustainable treatment: current status and future directions. *Discover Environment*, *3*(1): 132. https://doi.org/10.1007/s44274-025-00337-0

Mahlambi, M. M., Ngila, C. J., & Mamba, B. B. (2015). Recent Developments in environmental photocatalytic degradation of organic pollutants: The case of Titanium

Dioxide Nanoparticles—A Review. *Journal of Nanomaterials*, *2015*(1). https://doi.org/10.1155/2015/790173

Mandal, S., Calderon, J., Marpu, S. B., Omary, M. A., & Shi, S. Q. (2021). Mesoporous activated carbon as a green adsorbent for the removal of heavy metals and Congo red: Characterization, adsorption kinetics, and isotherm studies. *Journal of Contaminant Hydrology*, 243: 103869. https://doi.org/10.1016/j.jconhyd.2021.103869

Martínez-Huitle, C. A., Rodrigo, M. A., Sirés, I., & Scialdone, O. (2023). A critical review on latest innovations and future challenges of electrochemical technology for the abatement of organics in water. *Applied Catalysis B: Environmental,* 328: 122430. https://doi.org/10.1016/j.apcatb.2023.122430

Mohamadpour, F., & Amani, A. M. (2024). Photocatalytic systems: reactions, mechanism, and applications. *RSC Advances*, 14(29): 20609–20645. https://doi.org/10.1039/d4ra03259d

Oladoye, P. O., Bamigboye, M. O., Ogunbiyi, O. D., & Akano, M. T. (2022). Toxicity and decontamination strategies of Congo red dye. *Groundwater for Sustainable Development*, 19: 100844. https://doi.org/10.1016/j.gsd.2022.100844

Periyasamy, A. P. (2024). Recent advances in the remediation of Textile-Dye-Containing wastewater: prioritizing human health and sustainable wastewater treatment. *Sustainability*, 16(2): 495. https://doi.org/10.3390/su16020495

Saidi, M., Benomara, A., Mokhtari, M., & Boukli-Hacene, L. (2020). Sonochemical synthesis of Zr-fumaric-based metal-organic framework (MOF) and its performance evaluation in methyl violet 2B decolorization by photocatalysis. *Reaction Kinetics Mechanisms and Catalysis,* 131(2): 1009–1021. https://doi.org/10.1007/s11144-020-01897-3

Tian, Z., Li, G., Chen, X., Li, C., Liu, R., Yue, X., Peng, W., & Gu, H. (2025). Innovative lignin-based MOFs and COFs for biomedicine, energy storage, and environmental remediation. *Advanced Composites and Hybrid Materials*, *8*(1): 114. https://doi.org/10.1007/s42114-024-01201-0

Wang, Q., Gao, Q., Al-Enizi, A. M., Nafady, A., & Ma, S. (2019). Recent advances in MOF-based photocatalysis: environmental remediation under visible light. *Inorganic Chemistry Frontiers,* 7(2): 300–339. https://doi.org/10.1039/c9qi01120j

Yap, M. H., Fow, K. L., & Chen, G. Z. (2017). Synthesis and applications of MOF-derived porous nanostructures. *Green Energy & Environment*, 2(3): 218–245. https://doi.org/10.1016/j.gee.2017.05.003

Yasin, G., Kumar, A., Ali, S., Nguyen, T. A., & Ajmal, S. (2024). Multifunctional coordination materials for green energy technologies (1st ed.). Taylor & Francis. https://doi.org/10.1201/9781003345886

Zhang, S., Zhang, K., Xie, Y., Lou, Y., Lichtfouse, E., Feng, M., & Sharma, V. K. (2023). Ruthenium-driven catalysis for sustainable water decontamination: a review. *Environmental Chemistry Letters,* 21(6): 3377–3391. https://doi.org/10.1007/s10311-023-01642-x